A sheet on a drop reveals wrinkling and crumpling as distinct symmetry-breaking instabilities

Hunter King [*], **Robert D. Schroll** [*], **Benny Davidovitch** [*], **and Narayanan Menon** [*]

[*]Department of Physics, University of Massachusetts, Amherst, MA 01003

Submitted to Proceedings of the National Academy of Sciences of the United States of America

Smooth wrinkles and sharply crumpled regions are familiar motifs in biological or synthetic sheets, such as rapidly growing plant leaves and crushed foils. Previous studies have addressed both morphological types, but the generic route whereby a featureless sheet develops a complex shape remains elusive. Here we show that this route proceeds through an unusual sequence of distinct symmetry-breaking instabilities. The object of our study is an ultrathin circular sheet stretched over a liquid drop. As the curvature is gradually increased, the surface tension stretching the sheet over the curved drop causes compression along circles of latitude. The compression is relieved first by a transition into a wrinkling pattern, and then into a crumpled state via a geometry-driven continuous transition. Classical buckling theory describes wrinkling as a perturbation of the unbuckled state. However, our measurements prove that this textbook analysis fails for very thin sheets, and highlight the importance of a new, mechanical notion of "thinness" that is distinct from the geometric aspect ratio of the sheet. Our data provide the first conclusive evidence that the wrinkled state in ultra-thin sheets is described by a theory based on a compression-free, symmetric stress field. This insight leads to the surprising recognition that the wrinkle-to-crumple transition is not merely a further elaboration of the shape, but rather signals the symmetry-breaking of the stress field. Furthermore, our observations indicate that crumpling emerges through a continuous transition, where the imposed geometry frustrates the growth of wrinkles.

wrinkling and crumpling | phase transitions | instabilities

The richness and beauty of the patterns exhibited by a thin sheet may be viewed from the perspective of nonequilibrium pattern formation theory [1] which posits that morphological diversity emanates from successive instabilities of a highly-symmetric state. A simple example is the buckling of a sheet of paper compressed along two edges. The mechanics of this familiar Euler instability reflects the disparity between weak bending forces and strong compression forces, which becomes greater as the sheet gets thinner [2, 3]. Beyond the mechanical point of view, this instability can be recognized as a spontaneous breaking of the translation symmetry of the sheet in the confinement direction. The conceptual link between the Euler instability, symmetry breaking, and pattern formation, is more obvious when the sheet is placed under tension or is compressed on a soft substrate [4, 5]. This produces a periodic wrinkle pattern with a finite wavelength. The wrinkling pattern may be subject to secondary instabilities that break the translational symmetry further by introducing modes of larger wavelength [6, 7], or by superimposing on the wrinkles a localized fold shape [8, 9, 10]. This sequence of pattern development parallels that of prototypical driven systems such as Rayleigh-Benard convection and Taylor-Couette flow [1].

When sheets are subjected to a curved, 2-dimensional (2D) confinement [11, 12], new levels of shape complexity are obtained. Whereas the stress field is essentially uniform in the 1-dimensional (1D) examples above, it is spatially-varying and strongly coupled to the shape in 2D geometries. In this article, we study the sequence of patterns that develop when an ultrathin, circular sheet is placed on a fluid drop. The surface tension stretching the sheet over the curved drop leads to destabilizing compressive forces in the azimuthal direction. When the curvature of the drop is steadily increased, the axial symmetry of the initial geometry is first broken by a transition to a wrinkled state. In addition to the primary wrinkling instability, we discover yet another instability at higher curvature, in which the wrinkle pattern gives way to a state of lower azimuthal symmetry with localized crumpled features. Two unique features associated with this sequence sets it apart from the traditional progression of pattern formation theory: First, our measurements of the wrinkle extent provide the first conclusive evidence to a far-from-threshold (FFT) theory. This theoy describes the wrinkling of ultra-thin sheets as a perturbation about the compression-free limit of a sheet which can bend at no energetic cost [14, 15, 16], rather than through a perturbation about the unstable axisymmetric state [13], that is the basis of traditional near-threshold (NT) post-buckling methods. Second, we show that crumpling emerges through a continuous transition whereby the stress field, that presevres the axial symmetry of the system in FFT wrinkled state, spontaneously breaks this symmetry. This suggests that the wrinkle-to-crumple transition constitues a new type of morphological phase transition, that reflects a primary symmetry breaking of the force field rather than merely further lowering of the azimuthal symmetry of the shape. The puzzle associated with this transition is that despite its inherent mechanical character, the threshold for the transition is governed by purely geometric observables.

Experimental system

Our set-up is sketched in Fig. 1. A circular polystyrene sheet is delivered to the free surface of water at the top of a tube of radius 2.5 mm. The spin-coated sheet has thickness t from 49 to 137 nm and radius W of 0.79 or 1.5 mm. The tendency of the sheet to be flat is frustrated by the drop's desire to maintain a spherical shape. The shape of the exposed air-water interface shows no measurable deviations from a spherical cap with radius $R=2\gamma/P$, where γ is the liquid-vapor surface tension that stretches the sheet radially at its perimeter and P is a Laplace pressure that acts normal to its surface [1]. The pressure P is smoothly controlled by changing the height of a reservoir, and is measured with a precision of ± 1 Pa.

Imposing curvature on the sheet causes it to stretch and bend in the radial direction, but for sufficiently thin sheets

Reserved for Publication Footnotes

[1]We assume that gravity may be neglected, as the height of the drop is typically smaller than the capillary length.

stretching is much more energetically costly than bending. This basic property of elastic sheets is expressed through the different dependencies of the stretching and bending moduli, Y and B respectively, on the sheet's thickness: $Y = Et$, whereas $B = (E/12(1-\Lambda^2))t^3$. Here E is the Young's modulus ($E \approx 3.4\ GPa$ for PS) and Λ the Poisson ratio of the material.

A dimensionless group called *bendability* [17] can be defined as the ratio of the applied stretching force and the radial bending force:

$$\text{bendability:}\quad \epsilon^{-1} \equiv \gamma W^2/B\ . \qquad [1]$$

The bendability parameter incorporates mechanics (γ), in contrast to the purely geometric von Kármán number, $B/W^2Y \sim (t/W)^2$, which is the familiar measure of thinness.

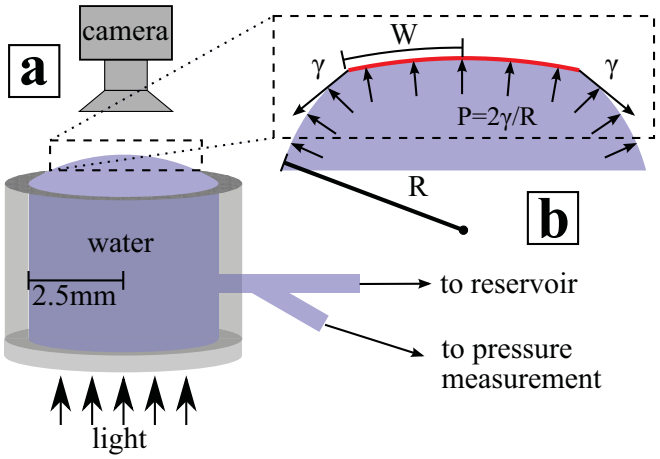

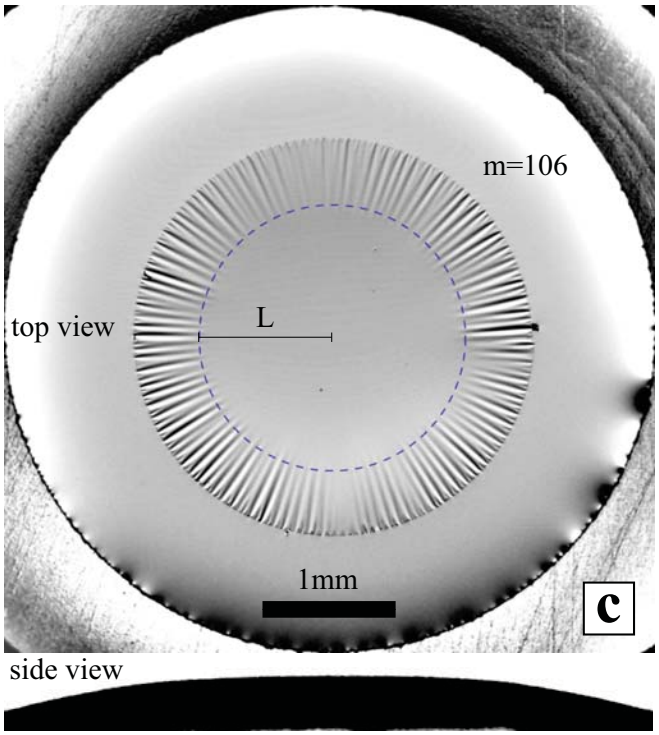

Fig. 1. (a) Experimental set-up. (b) Schematic side view of the drop and sheet. The sheet has radius W and the exposed part of the drop beneath has radius of curvature R. (c) Top and side views of the wrinkled sheet on the drop. The radius of the unwrinkled region (L) and the wrinkle angle ($\frac{2\pi}{m}$) are computed by analyzing the top image (SI.7).

This parameter differentiates our system from the "capillary origami" experiment [12], where thicker sheets were used to wrap fluid droplets. For those low bendability films, bending forces can balance the drop's pressure. By contrast, we use ultrathin highly-bendable sheets where $\epsilon < 5{\cdot}10^{-6}$. The dominance of stretching over bending forces in this regime suggests that the shape is governed by the balance of elastic stresses in the sheet and the resisting force of the drop to deviate from its favoured sphericity.

Theory

We distinguish between two types of axisymmetric states: (i) If the sheet is small and the exerted tension (γ) is strong, the stress will be tensile everywhere in the sheet in both radial and hoop (azimuthal) directions. This case, where the drop is only slightly deformed, is similar to radial stretching of an unsupported sheet, and the drop's curvature has only a small effect. (ii) However, if the sheet is sufficiently large or the tension sufficiently weak, the hoop stress becomes compressive in an annulus $L < r < W$ close to its outer edge, signifying a wrinkling instability of the axisymmetric state. Here, the drop's curvature has an effect similar to projecting a flat sheet onto an undeformable sphere, where the confinement of circles of latitude increases with their radius. This qualitative discussion suggests that the onset of wrinkling in a highly bendable sheet on a drop is dominated by a "confinement" parameter that increases with the radius W of the sheet and decreases with increasing tension γ.

A quantitative analysis of the axisymmetric state [18] is based on the Föppl–von Kármán (FvK) equations that express force balance in the radial and normal directions:

$$\text{radial:}\quad d(r\sigma_{rr})/dr - \sigma_{\theta\theta} = 0 \qquad [2]$$

$$\text{normal:}\quad B\triangle_r{}^2\zeta - \sigma_{rr}d^2\zeta/dr^2 - \sigma_{\theta\theta}r^{-1}d\zeta/dr = P \qquad [3]$$

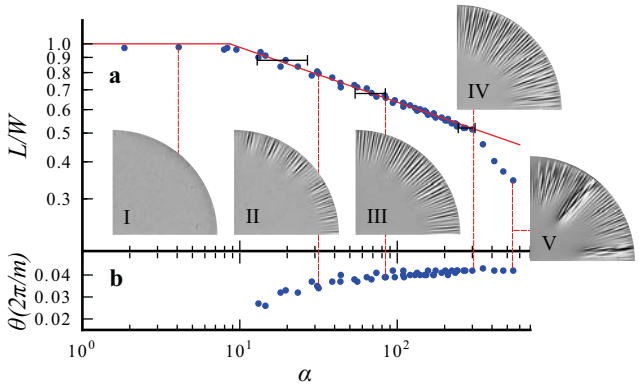

Fig. 2. (a) Radius of the unwrinkled region L, scaled by the sheet's radius W and (b) average angle between wrinkles $360/m$ (m is the wrinkle number), for a sheet of thickness $t = 77\ nm$ and radius $W = 1.5\ mm$. Consecutive data points are taken by increasing the drop's curvature R^{-1}. The x-axis is the confinement parameter $\alpha = YW^2/2\gamma R^2$. A top view of the sheet is shown at several representative values of α (dashed lines connect images to corresponding data points). No hysteresis is seen in the observed patterns until extremely high curvature, when the sheet begins to make self-contacts.

[2] FvK theory assumes a Hookean, linear response which requires small strains everyehere. For axisymmetric stress fields, this limits our analysis to small slope ($|\zeta'(r)| \ll 1$), and hence $W/R \ll 1$. Nevertheless, the ratio W/R appears only in the confinement $\alpha = (Y/2\gamma)(W/R)^2$, hence the regime $W/R \ll 1$ is realized for sufficiently small tensile strains ($\gamma/Y \sim (W/R)^2 \ll W/R \ll 1$). See also SI.5.

where $\sigma_{rr}(r), \sigma_{\theta\theta}(r)$ are, respectively, the radial and hoop stress components, $\zeta(r)$ is the normal displacement of the sheet, and $\triangle_r = r^{-1}\frac{d}{dr}(r\frac{d}{dr})$. In the high bendability regime, $\epsilon \ll 1$, the bending force ($\sim B$) in Eq. (3) is neglected. In Supplementary Information, Sec. 3 (SI.3) we show that Eqs. (2,3) imply a dependence of the axisymmetric state on a single dimensionless group that does match the form of the confinement parameter anticipated by the above argument:

$$\text{confinement:}\ \ \alpha \equiv YW^2/2\gamma R^2\ . \qquad [4]$$

Our numerical analysis of Eqs. (2,3) predicts a critical value $\alpha^0_{wr} \approx 5.16$, such that for $\alpha < \alpha^0_{wr}$ the sheet is everywhere stretched, whereas for $\alpha > \alpha^0_{wr}$ the hoop stress becomes compressive at $r > L_{\rm NT}(\alpha)$, and reaches a maximal compression at the perimeter $\sigma_{\theta\theta}(W) \sim -\gamma(\alpha - \alpha^0_{wr})$ (Fig. SI3(b), [2]). The predicted function $L_{\rm NT}(\alpha)$ is plotted in Fig. 3a (dashed black). Since a sheet with finite bending modulus can support some compression without buckling, the axisymmetric state becomes unstable at some threshold $\alpha_{wr}(\epsilon)$ that is expected to approach α^0_{wr} as $\epsilon \to 0$. A traditional buckling analysis [13] considers the wrinkling state as a perturbation of the axisymmetric state. However, since the axisymmetric reference state experiences a compression $\sigma_{\theta\theta} \sim -\gamma(\alpha - \alpha^0_{wr})$, which cannot be supported by very thin sheets, the validity of this standard perturbation method in the high bendability regime, $\epsilon \ll 1$, is expected to be limited to confinement values that are only slightly above $\alpha_{wr}(\epsilon)$ [17].

An alternative, far-from-threshold (FFT) approach [17] for characterizing wrinkling patterns in highly bendable sheets, consists of a perturbation theory around the so-called "membrane limit" of a sheet with zero bending modulus (but finite stretching modulus) [14, 15, 16]. In this singular limit, wrinkles do not cost any bending energy, and the compression can be completely relaxed by generating infinitely many wrinkles.

The FFT theory [17] proceeds in two steps (SI.2, [17]): *(i)* Finding the asymptotic stress field of the system in the "membrane limit" by solving Eqs. (2,3) under the constraint that the stress field is compression-free (i.e. $\sigma_{\theta\theta} \geq 0$) [14]. Notably, the stress field remains axisymmetric in the FFT wrinkled state even though the wrinkles break the symmetry of the shape. The compression-free stress field determines the FFT extent of wrinkles $L_{\rm FFT}$. *(ii)* Determining the number of wrinkles, $m_{\rm FFT}$, from a perturbation theory around the membrane limit. The distinct nature of the reference stress fields results in markedly different predictions for the extent and number of wrinkles in the NT and FFT regimes, as we explain in detail in SI.4. We found the following predictions for the normalized extent of the unwrinkled zone $\tilde{L} = L/W$, and the number of FFT wrinkles:

$$\tilde{L}_{\rm FFT}(\alpha) = \sqrt[5]{(\alpha^0_{wr}/\alpha)}\ \ ;\ \ m_{\rm FFT} \approx k(\alpha)\ \epsilon^{-1/4}\ . \qquad [5]$$

The predicted extent of the FFT wrinkles is plotted in Fig 3A (solid black). The scaling law for the wrinkle number is similar to the one discovered by Cerda and Mahadevan [5] for stretched rectangular sheets.

Experimental results and discussion

In Fig. 2a we show a set of images (I-V) that from left to right indicate the patterns obtained upon increasing the pressure of the droplet. The sheet first smoothly stretches (I), and then starts wrinkling at the edge (II). The wrinkles grow toward the center of the sheet and increase modestly in number (III). Further in the progression, some of the wrinkles develop sharp cusp-like patterns (IV). Finally, most of the original wrinkles recede, leaving a few sharply defined crumpled features (V) that are approximately uniformly distributed around the sheet. (Higher resolution images, and the corresponding side views are available in SI.7)

This progression is quantitatively characterized in terms of $\tilde{L}$, the fractional extent of the unwrinkled zone in the interior of the sheet, and $2\pi/m$, the average angle between wrinkles. Both are plotted as functions of the confinement α for a sheet with thickness $t = 77\ nm$. Fig. 2 shows that wrinkles emerge at a sharply defined value, α_{wr}. The wrinkles grow inward for $\alpha > \alpha_{wr}$ in excellent agreement with the power law $\tilde{L} \sim \alpha^{-1/5}$ predicted by the FFT analysis, Eq. (5), over about 1.5 decades of confinement values α. Over the same range, the number of wrinkles increases slightly as shown in the lower panel. From similar plots of $\tilde{L}$ for other sheets, we obtain values of α_{wr} that vary between 3 and 11 from sample to sample. This range includes the predicted value $\alpha^0_{wr} = 5.16$, and there is no systematic dependence of the measured α_{wr} on t and L.

For $\alpha \gtrsim \alpha_{cr} \approx 30\alpha_{wr}$, a deviation is seen from the power law scaling of the length, at approximately the same values of pressure at which sharp, crumple-like features begin to appear at the tips of some wrinkles. It is difficult to pinpoint the exact value α_{cr} at which these features appear, but beyond this value, we show in Fig. 2 the length of the leading crumples, and the separation angle of all remaining wrinkled or crumpled features.

In Fig. 3a, we once again show the extent of the unwrinkled zone, but for a number of sheets of varying thickness

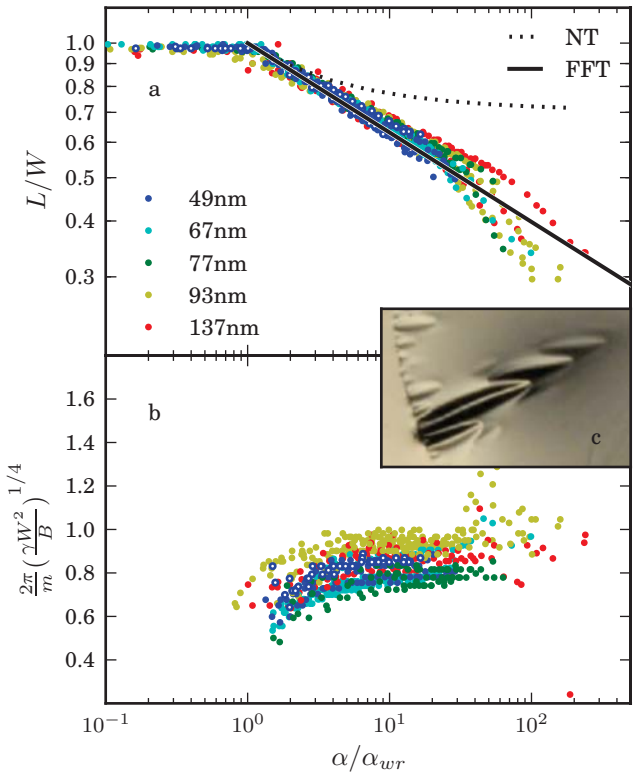

Fig. 3. (a-b) Normalized radius of the unwrinkled region L/W, and wrinkle angle are plotted similarly to Fig. 2, but for a range of thicknesses ($49 - 137\ nm$) and two radii: $0.79\ mm$ (○) and $1.5\ mm$ (●). The x-axis is now the rescaled confinement parameter α/α_{wr}, where the denominator is the measured value at the wrinkling threshold. The wrinkle angle (in b) is scaled by $(W^2\gamma/B)^{1/4}$. Fig. 3a shows a good agreement of the wrinkle extent with the FFT prediction (solid line) over a factor of about 30 in α; the NT prediction (dashed line) departs from the data beyond threshold. (c) A close-up view of a crumpled structure obtained at large α.

and size, now plotted against the scaled confinement parameter α/α_{wr}, where α_{wr} is the measured value at the wrinkling threshold. The data for all thicknesses collapse well for $\alpha < \alpha_{cr}$, indicating that the length of the wrinkles is independent of the bendability ϵ^{-1} as anticipated in the FFT theory. There is no regime of α in which the NT behaviour (indicated in Fig.3a by a dashed line) is seen, an absence consistent with the high bendability values of the sheets used here (ϵ^{-1} varies from $2 \cdot 10^4$ to $5 \cdot 10^6$).

In Fig. 3b we show a similar plot of the wrinkle separation angle $2\pi/m$ scaled by the anticipated FFT dependence of $\epsilon^{-1/4}$, Eq. (5). The bendability ϵ^{-1} thus affects the scaling of the wavelengths of the wrinkling pattern [5, 20], but not the stretching energies that control the wrinkle extent [17]. A detailed numerical prediction for the wrinkle angle is not yet available (SI.2,SI.4, [17]), but the data collapse suggests that the wrinkle number m depends only weakly on α.

As Fig. 3a shows, the deviation from the power law scaling becomes evident for $\alpha > \alpha_{cr} \approx 30\ \alpha_{wr}$. The spread in the angle and length data beyond this value reflects the complexity of the crumpled state (Fig. 2a.V) that ultimately replaces the wrinkling pattern. A representative localized shape (Fig. 3c) shows that one of the motifs of the crumpled state has the shape of a developable cone ("d-cone") which is a fundamental stress-focused element seen in thin sheets [3]. The emergence of these localized structures strongly modifies the overall shape of the drop and sheet: the broken azimuthal symmetry of the wrinkling pattern gives way to an even lower symmetry polygonal shape.

We propose that crumpling emerges from an instability of wrinkling upon large confinement. Thus a proper description of the crumpling transition requires a nonlinear, FFT description of the wrinkled state. The continuous deviation of $\tilde{L}$ from the predicted FFT wrinkle extent (Fig. 3a) and the gradual emergence of focused structures from the tips of wrinkles suggests that the crumpling transition is of second order [1]. Furthermore, the apparently continuous nature of the crumpling transition is intimately related to the symmetry-breaking nature of this transition. As our theoretical discussion emphasized, the FFT wrinkling solution of FvK equations makes the two distinct assumptions of a vanishing compressive stress, and an axisymmetric stress field. While we expect the first of these assumptions to be valid also in the crumpled state, stress focusing is obviously incompatible with axial symmetry. We thus conclude that wrinkling is a primary instability that breaks the axial symmetry of the pattern but not of the stresses, whereas crumpling emerges from a nonstandard secondary instability that breaks the axial symmetry of the stress field rather than just producing a lower level of azimuthal symmetry in the shape.

In the crumpled state, our measurements show a spread in the scaled extent and angle that is not collapsed by the scaled confinement α/α_{wr}. However, we observe (Fig. 3a) that the onset of the crumpling transition seems to occur when the radius of the unwrinkled zone shrinks to about a half the sheet radius $\tilde{L} \approx 0.5 \pm 0.02$ [3]. We recall that the wrinkling transition occurs at α_{wr}, which is controlled by both mechanics (Y, γ) and geometric length scales (W, R). The observation that the crumpling transition occurs when an emergent length scale L becomes a finite fraction of the sheet's radius W leads us to infer that this transition is geometric in origin. The wrinkles can no longer minimize elastic energy efficiently, and a broken-symmetry, localized stress-field becomes the favoured state.

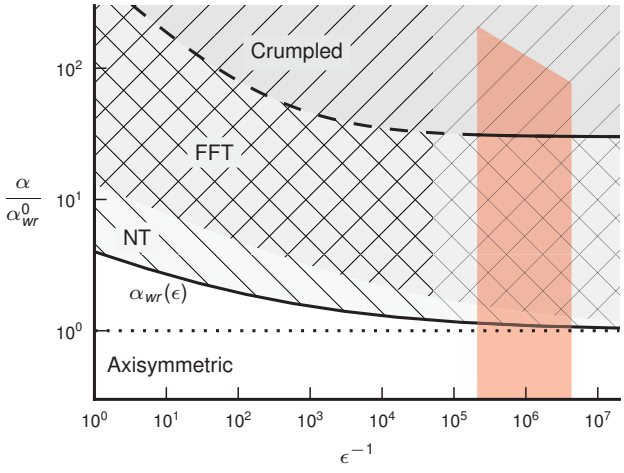

Fig. 4. A schematic phase diagram for the morphology of an ultrathin sheet on a drop, spanned by the confinement (α) and bendability (ϵ^{-1}) parameters. The shaded area corresponds to the experimental parameter regime. The axisymmetric state is unstable above a critical curve $\alpha_{wr}(\epsilon)$ (solid line) that approaches α^0_{wr} as $\epsilon \to 0$. A FFT theory describes the wrinkling pattern for confinement values that become indefinitely close to $\alpha_{wr}(\epsilon)$ in the high bendability limit $\epsilon \to 0$. The FFT wrinkling pattern transforms into a crumpled shape for sufficiently large confinements $\alpha > \alpha_{cr}$. This transition is observed to be governed by the geometric rule $\tilde{L} \approx 1/2$. Hence, the transition to crumpling does not have a universal description in terms of α and ϵ. The wrinkling transition and FFT description are similar to those predicted for planar axisymmetric stretching [17], but a crumpling transition is not seen in that geometry.

Conclusions

Confinement of a sheet on a deformable sphere leads to a richness of form that is useful to view through the lens of pattern development theory. Our observations and analysis suggest the schematic phase diagram plotted in Fig. 4. The sheet is unwrinkled for low confinement values, $\alpha < \alpha_{wr}(\epsilon)$. For the ultrathin, highly-bendable sheets we use in this study, the NT wrinkled regime occupies only a tiny sliver of the phase diagram. As is evidenced by our measurements of the extent and number of wrinkles, the FFT scenario becomes operative even at confinement values that are only slightly above threshold. This result emphasizes the importance of the correct application of FFT behaviour to the many modern applications that use sheets of nanoscopic dimensions as mechanical elements.

Our study demonstrates the generality of the bendability and confinement parameters, which were first proposed for the Lamé geometry of a thin annular sheet under axisymmetric radial tension gradient [17]. An important advantage of our system is the ability to test the scaling of wrinkle length for confinements much larger than the threshold value, whereas experiments in the planar, Lamé geometry are limited to no more than 2-3 times the threshold value [19, 20, 17]. We stress that despite their central role, we do not expect bendability and confinement to be the only morphologically-relevant parameters of elastic sheets, since they cannot capture patterns induced by substrate stiffness and boundary effects. Appropriate substrate parameters will be required to characterize basic types of instabilities, such as folding in floating sheets [8, 21], "period-doubling" [7] and "n-tupling" [6] in sheets on elastomers, and a subcritical creasing instability in neo-Hookean solids [22, 23]. Likewise, boundary forces not encoded in ϵ and α have been observed to drive multiscale wrinkling cascades [24, 25].

[3] In SI.5 we explain why deviations of L_{FFT} from the solid line in Fig. 3a are consistent with FFT analysis.

As far as we are aware, our study provides the first experimental scenario that exhibits a controlled transition between wrinkled and crumpled shapes. This second instability of a highly-symmetric, featureless state is associated with a primary symmetry breaking of the stress field. The data indicate a continuous transition determined by the inherent frustration of the geometry rather than by mechanical forces. Analogous studies of 2D crystals on droplet surfaces [26, 27] show that point and line lattice defects may also resolve geometric frustration. The relationship between those defects and the localized structures emerging from a continuum remain to be explored. While our motivation in choosing a spherical substrate was to frustrate the sheet at all points in space, it is not clear that this was a necessary ingredient to achieve crumpling. 1D patterns do not appear to crumple, and neither do all 2D geometries [19, 20, 17]. It remains a puzzle as to what the generic conditions are under which a wrinkled state gives way to crumpling.

Materials and Methods

Apparatus. The tube depicted in Fig. 1 was set in a hole through an acrylic base. The hole was sealed on the bottom by a glass slide to keep the setup watertight and transparent to allow illumination from beneath. The surface was silanized in order to pin the contact line at the inner diameter of its top edge. Also fixed in the base were 4mm and 3mm silanized glass tubes, set at two different heights, both lower than the center tube. All these tubes were connected to a reservoir on an adjustable vertical stage. The pressure in the tube containing the sample is measured with a precision of $\pm 1 Pa$ by measuring the air-water meniscus in the other two tubes (see SI.6).

Film preparation. Films were prepared by spin-coating from a dilute solution of polystyrene in toluene (PS: atactic, number-average molecular weight $Mn = 91\ K$, weight-average molecular weight $Mw = 95\ K$, purchased from Polymer Source Inc.) on glass substrates. Different film thicknesses were obtained either by varying spin speed (between 800 and 2000 RPM) or the concentration of polystyrene in solution (between 1% to 2% by mass). Circular cuts of radius $W =$ 0.79 or 1.5 mm were made in the film. The circular film was released on to an air-water interface and then transferred onto the experimental set-up (see SI.6). The thickness was measured with a precision of 0.2 nm using a Filmetric white-light interferometer, and was uniform to ± 1 nm over the area of the film.

Images. Two types of raw data were collected: top-view photographs, in which features of the film could be measured, and side-view photographs of the menisci of the three fixed tubes, from which the pressure under the film could be calculated. The top-view photographs were taken by a Nikon D5000 dSLR camera equipped with a bellows unit for macrophotography. The camera was attached to a microscope base which provided light from below. Contrast in the images convey the local slope of the film-air interface. The intensity as a function of angle was analyzed at all radial positions in order to determine wrinkle length and wrinkle angle (see SI.7).

ACKNOWLEDGMENTS. We thank P. Buchak and G. Farrell for useful conversations; K.B. Toga, J. Huang, and P. Zheng for technical help; N. Shoresh for comments on the manuscript. This work was supported by NSF-DMR-0907245 (H.K and N.M), NSF-MRSEC at UMass Amherst (R.D.S and instrumentation facilities), and the Petroleum Research Fund of the American Chemical Society (B.D.).

1. Cross M, Greenside H (2009) Pattern formation and dynamics in nonequilibrium systems (Cambridge University Press, Cambridge, UK).
2. Landau L-D, Lifshitz E-M (1986) Theory of elasticity 3^{rd} Edition (Butterworth-Heinemann, UK).
3. Witten T-A (2007) Stress focusing in elastic sheets. Rev. Mod. Phys. 79: 643-675.
4. Bowden N et al. (1998) Spontaneous formation of ordered structures in thin films of metals supported on an elastomeric polymer. Nature 393: 146-149.
5. Cerda E, Mahadevan L (2003) Geometry and physics of wrinkling. Phys. Rev. Lett. 90: 074302.
6. Efimenko K et al. (2005) Nested self-similar wrinkling patterns in skins. Nature Materials 4: 293-297.
7. Brau F et al. (2011) Multiple-length-scale elastic instability mimics parametric resonance of nonlinear oscillators. Nature Physics 7: 56-60.
8. Pocivavsek L et al. (2008) Stress and fold localization in thin elastic membranes. Science 320:912-916.
9. Diamant H, Witten T-A (2011) Compression Induced Folding of a Sheet: An Integrable System. Phys. Rev. Lett. 107:164302.
10. Audoly B (2011) Localized buckling of a floating elastica. Phys. Rev. E 84: 011605.
11. Hure J, Roman B, Bico J (2011) Wrapping an Adhesive Sphere with an Elastic Sheet. Phys. Rev. Lett. 106:174301.
12. Py E et al. (2007) Capillary Origami: Spontaneous wrapping of a droplet with an elastic sheet. Phys. Rev. Lett. 98:156103.
13. Timoshenko S-P and Goodier J-N (1970) Theory of Elasticity (McGraw Hill, New-York).
14. Stein M and Hedgpeth J-M (1961) Analysis of Partly Wrinkled Membranes. (NatlAeronau- tics Space Admin, Washington) Technical Note D-813.
15. Pipkin A-C (1986) The relaxed energy density for isotropic elastic membranes. IMA J. App. Math. 36:85-99.
16. Mansfield E-H (1989)The Bending and Stretching of Plates (Cambridge University Press, Cambridge, UK).
17. B. Davidovitch et al. (2011) Prototypical model for tensional wrinkling in thin sheets. Proc. Nat. Acad. Sci. 108: 18227-18232.
18. Vella D, Adda-Bedia M, Cerda E (2010) Capillary wrinkling of elastic membranes. Soft Matter 6:5778-5872.
19. Géminard J-C, Bernal R, Melo F (2004) Wrinkle formations in axi-symmetrically stretched membranes. Eur. Phys. J. E 15:117-126.
20. Huang J et al. (2007) Capillary wrinkling of floating thin polymer films. Science 317:650-653.
21. Holmes D-P, Crosby A-J (2010) Draping films: A wrinkle to fold transition. Phys. Rev. Lett. 105:038303.
22. Hohlfeld E, Mahadevan L (2011) Unfolding the Sulcus. Phys. Rev. Lett. 106:105702.
23. Trujillo V, Kim J and Hayward R-C (2008) Creasing instability of surface-attached hydrogels. Soft Matter 4:564-569.
24. Huang J et al. (2010) Smooth cascade of wrinkles at the edge of a floating elastic film. Phys. Rev. Lett. 105:038302.
25. Vandeparre H et al. (2011) Wrinkling hierarchy in constrained thin sheets from suspended graphene to curtains. Phys. Rev. Lett. 106:224301.
26. Irvine W-T-M, Vitelli V and Chaikin P-M (2010) Pleats in crystals on curved surfaces. Nature 468:947-951.
27. Bausch A-R et al. (2003) Grain boundary scars and spherical crystallography. Science 299:1716-1718.